XVIII International Conference on Water Resources
CMWR 2010
J. Carrera (Ed)
CIMNE, Barcelona 2010

COMPARISON OF CELL-CENTERED AND NODE-CENTERED FORMULATIONS OF A HIGH-RESOLUTION WELL-BALANCED FINITE VOLUME SCHEME: APPLICATION TO SHALLOW WATER FLOWS

A.I. Delis[*], I.K. Nikolos[†] and M. Kazolea[††]

[*] Department of Sciences, Technical University
University Campus, Chania, Crete, 73100, Greece
e-mail: adelis@science.tuc.gr, web page: http://www.science.tuc.gr

[†] Department of Production Engineering & Management, Technical University of Crete
University Campus, Chania, Crete, 73100, Greece
e-mail:jnikolo@dpem.tuc.gr

[††] Department of Environmental Engineering
University Campus, Chania, Crete, 73100, Greece
e-mail:mkazolea@isc.tuc.gr

Key words: Shallow water equations, cell-centered and node-centered finite volumes, MUSCL, source terms; wet-dry fronts.

Summary. We present numerical comparisons for the simulation of unsteady 2D shallow water flows over topography with wet/dry fronts, between well-balanced cell-centered and node-centered formulations of a finite volume high-resolution algorithm. In both formulations we utilize Roe's Riemann solver, while second-order spatial accuracy is achieved with MUSCL-type reconstruction techniques. Grid refinement studies are emphasized.

1 INTRODUCTION

The current-day unstructured mesh 2D hydrodynamics codes rely, almost exclusively, on formally second order accurate FV discretizations in order to approximate numerically the 2D non-linear shallow water equations (NSWE). The NSWE are accepted to mathematically describe a wide variety of free surface flows under the effect of gravity. FV schemes can be categorized, in the main, as of the *cell-centered* or the *node-centered* type. For the CCFV approach, the volumes used to satisfy the integral form of the equation are the mesh elements (triangles) themselves while for the NCFV approach the volumes are elements of the mesh dual to the primal computational mesh.

Any numerical approach for the approximation of the NSWE should embody the following necessary properties: be of high-order accuracy (in space and time); has the ability of simulating discontinuous flows accurately; be conservative; enable various practical

inflow/outflow conditions; incorporate complex topography and has the ability of modeling moving wet/dry interfaces. The satisfaction of the last two properties constitute particular challenging problems for all numerical methods. Great research effort has been recently devoted in deriving FV schemes on unstructured meshes that resolve numerically these problems, we refer to[1,2] and references therein. With regard to the first problem, several numerical and mathematical treatments have been proposed in the literature for balancing the flux gradient and the source terms in order to properly compute stationary or almost stationary solutions. This property is known as *well-balancing*. Both FV approaches considered in this work can be considered as state of the art for the given flow problems and incorporate all the latest technology in properly treating the above mentioned problems and satisfy all the desired properties mentioned above. Relative advantages of each of the two approaches have been presented in the literature but there exists no consensus about which approach offers more advantages. One of the difficulties in assessing the two approaches is that, comparative calculations in a controlled environment, i.e., computations from the same codes, same degrees of freedom, computational parameters and comparisons on the same test problems, to the best of our knowledge, do not exist. Results should be compared to analytical solutions or experimental data, or at least compared to computational results obtained independently. In addition, grid dependence in the solution should always be reported.

In this work, we provide a controlled environment for a fair and extensive comparison between the two approaches. Grid refinement studies are emphasized on 2D grids range from regular triangular grids to irregular ones. The main targets in this work are: (i) to rigorously verify the robustness and accuracy of the presented FV formulations and (ii) to carefully study the relative performance of the two approaches in order to draw fair and firm conclusions in terms of applicability and performance.

2 THE SHALLOW WATER SYSTEM OF EQUATIONS

The well-known system of the 2D NSWE written in conservation law form read:

$$\frac{\partial \mathbf{U}}{\partial t}+\nabla\cdot\mathbf{H}\left(\mathbf{U}\right)=\mathbf{L}\left(\mathbf{U},x,y\right)\ \text{on}\ \Omega\times\left[0,t\right]\subset\mathbb{R}^2\times\mathbb{R}^+ \tag{1}$$

where we have

$$\mathbf{U}=\begin{bmatrix} h \\ hu \\ hv \end{bmatrix},\qquad \mathbf{H}\left(\mathbf{U}\right)=\begin{bmatrix}\mathbf{F} & \mathbf{G}\end{bmatrix}=\begin{bmatrix} hu & hv \\ hu^2+\frac{1}{2}gh^2 & huv \\ huv & hv^2+\frac{1}{2}gh^2 \end{bmatrix}, \tag{2}$$

with $\mathbf{u}=\left[u,v\right]^{\mathrm{T}}$ the velocity field, g the gravitational acceleration, $h\left(x,y,t\right)\geq 0$ the flow depth. The source term $\mathbf{L}\left(\mathbf{U}\right)=\left[\mathbf{R}+\mathbf{S}\right]$ models the effects of the shape of the topography and friction on the flow. By denoting with $B\left(x,y\right)$ the bed topography elevation (therefore $H=h+B$ is the water free surface level), the geometrical source term is given as $\mathbf{R}=\mathbf{R}_x^b+\mathbf{R}_y^b$ where

$$\mathbf{R}_x^b = \begin{bmatrix} 0 & -gh\dfrac{\partial B(x,y)}{\partial x} & 0 \end{bmatrix}^{\mathrm{T}}, \quad \mathbf{R}_y^b = \begin{bmatrix} 0 & 0 & -gh\dfrac{\partial B(x,y)}{\partial y} \end{bmatrix}^{\mathrm{T}}, \tag{3}$$

The source term component $\mathbf{S}$ includes the bed friction stresses, given as,

$$\mathbf{S} = \begin{bmatrix} 0 & -ghS_x^f & -ghS_y^f \end{bmatrix}^{\mathrm{T}} \text{ with } S_x^f = \frac{n_m^2 u\|\mathbf{u}\|}{h^{4/3}} \text{ and } S_y^f = \frac{n_m^2 v\|\mathbf{u}\|}{h^{4/3}}, \tag{4}$$

where S_x^f and S_y^f are the friction loss slopes and n_m the Manning roughness coefficient.

3 GRID TERMINOLOGY AND THE FINITE VOLUME FORMULATIONS

An initial conforming triangulation of $\Omega \subset \mathbb{R}^2$ composes the so-called *primal mesh*. The *median-dual* partition is used to generate control volumes for the NCFV scheme. For the CCFV the primary triangular cells serve as control volumes. The locations of discrete solutions are called *data points* while the cell boundaries are called *faces* and the term *edge* refers to the line connecting the neighboring data points. The grids used can be classified as *regular* or *irregular* ones. Four types of grids are considered here: (I) Equilateral triangular; (II) Regular triangular, derived from quadrilateral grids where cells are divided by the diagonals in four cells; (III) Regular triangular grids derived from quadrilateral grids by the same diagonal splitting; and (IV) Randomly perturbed (distorted) grids, generated by perturbing the grid nodes, of a type-(I) equilateral grid, from their original positions by random shifts. The representative grid types are shown in Fig. 1.

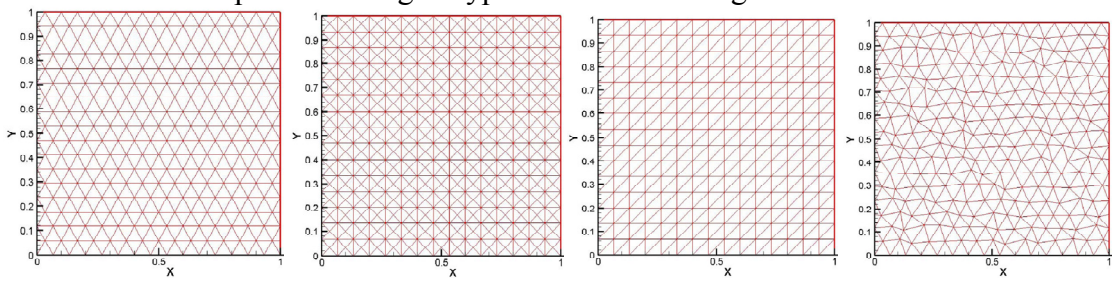

Figure 1: Grid Types (I to IV)

The major requirement, in order to perform convergence studies and fair comparison between the two types of schemes, for a sequence of refined grids is to satisfy the *consistency refinement property*[8]. This property requires the maximum distance across the grid cells to decrease consistently with increase of the total number of grid data points *N*. In particular the maximum distance should tend to zero as $N^{-1/2}$. As such, this property enables meaningful assessment of the asymptotic order of convergence. For a given computational domain, and without loss of generality, with dimensions $L_x \times L_y$ we define a subdivision of L_x by N_x line segments, $\Delta x = L_x / N_x$. As such, we define the characteristic length for each grid as $h_N = \sqrt{\left(L_x \times L_y\right)/N}$. For a consistently refined grid we half Δx and it follows that, for the new refined grid $h'_N \simeq h_N/2$ and $N' \simeq 4N$. For a fair comparison between NCFV and CCFV

schemes we need to derive *equivalent meshes* based on the degrees of freedom i.e. grid data points N. As such, equivalent grids can be defined as those having the same h_N, keeping in mind that for a CCFV scheme N corresponds to the number of triangular cells in the mesh while for a NCFV scheme to the mesh nodes.

Both FV schemes constructed in this work are based on the integral form of (1) over a general computational domain Ω:

$$\frac{\partial}{\partial t}\iint_{\Omega}\mathbf{U}d\Omega+\iint_{\Omega}\left(\nabla\cdot\mathbf{H}\right)d\Omega=\iint_{\Omega}\mathbf{L}d\Omega\,. \tag{5}$$

By application of Gauss's divergence theorem to the flux integral and denoting $\mathbf{U}_I$ the average value of the conserved quantities over the volume at a given time, from equation (5) the following conservation equation can be written for every I-cell

$$\frac{\partial\mathbf{U}_I}{\partial t}=-\frac{1}{|\Omega_I|}\oint_{\Gamma_I}\left(\mathbf{F}\tilde{n}_x+\mathbf{\Gamma}\tilde{n}_y\right)d\Gamma+\frac{1}{|\Omega_I|}\iint_{\Omega_I}\mathbf{L}d\Omega\,, \tag{6}$$

where $\tilde{\mathbf{n}}=\left[\tilde{n}_x,\tilde{n}_y\right]^{\mathrm{T}}$ is the outward unit normal vector, and I becomes P for the NCFV and p for the CCFV, as depicted in Fig. 2.

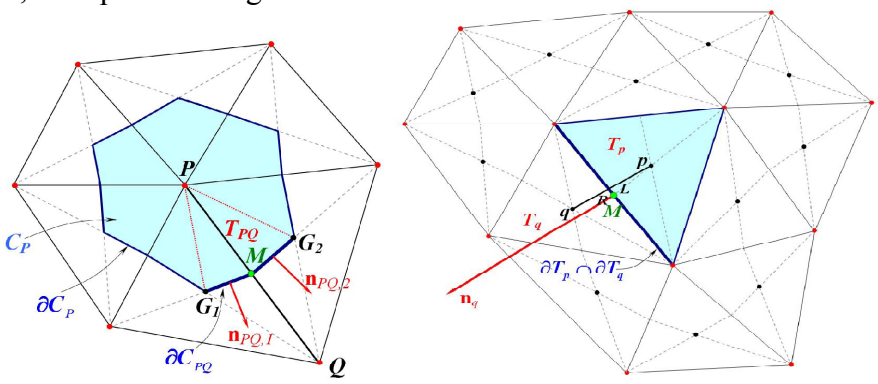

Figure 2: NCFV (left) and CCFV (right) control volumes

Additionally, Ω_I and Γ_I become C_P and ∂C_P for the NCFV and T_p and ∂T_p for the CCFV respectively. By introducing the numerical flux vectors $\mathbf{\Phi}$ and topography contribution term $\mathbf{\Psi}$ at midpoints M (Fig. 2), the semi-discrete form of (6) becomes:

$$\frac{\partial\mathbf{U}_I}{\partial t}=-\frac{1}{|\Omega_I|}\sum_k\mathbf{\Phi}_k-\frac{1}{|\Omega_I|}\sum_k\mathbf{\Phi}_{k,bound}+\frac{1}{|\Omega_I|}\sum_k\mathbf{\Psi}_k\,, \tag{7}$$

where k becomes $Q\in K_P$, the set of neighboring nodes to P for NCFV, and $q\in K_p, K_p:=\left\{q\in\mathbb{N}\middle|\partial T_p\cap\partial T_q\ is\ a\ face\ of\ T_p\right\}$ for the CCFV. The numerical flux is computed using the well-known Roe's approximate Riemann solver[2,3,4], while topography source vectors are discretized in an upwind fashion, as to satisfy the C-property[5,4,2].

Second order spatial accuracy is achieved in both formulations using a MUSCL-type

reconstruction, combined with the Van Albada edge-type slope limiter[2]. For the NCFV the reconstructed variables at the midpoint of edge PQ are:

$$w_{PQ}^{L} = w_P + \frac{1}{2} LIM\left(\mathbf{r}_{PQ} \cdot \nabla w_P\right),\ w_{PQ}^{R} = w_Q - \frac{1}{2} LIM\left(\mathbf{r}_{PQ} \cdot \nabla w_Q\right). \tag{8}$$

The gradient is computed using the Green-Gauss linear reconstruction and the stencil of Fig. 3, with an edge-based formulation[2]. For the CCFV formulation, using a similar approach, by projecting along the line connecting the volume centers, the reconstructed variables are given (taking into account that we wish to use the same edge-type slope limiter):

$$w_{D,p}^{L} = w_p + LIM\left(\mathbf{r}_{pD} \cdot \nabla w_p\right),\ w_{D,q}^{R} = w_q - LIM\left(\mathbf{r}_{Dq} \cdot \nabla w_q\right), \tag{9}$$

where D is the intersection point of face $\partial T_p \cap \partial T_q$ with $\overline{pq}$, which in general does not coincide with M. For this reason a novel correction is applied in this work to correct this inconsistency, which is responsible for a decrease in the order of convergence for type of grids where the distance between D and M is large. Eq. (9) then reads (Fig. 4):

$$w_p^{L} = w_{D,p}^{L} + \mathbf{r}_{DM} \cdot \nabla w_p,\ w_q^{R} = w_{D,q}^{R} + \mathbf{r}_{DM} \cdot \nabla w_q\ . \tag{10}$$

For the CCFV two different stencils are used for the Green-Gauss linear gradient computation, the compact one, that uses only the three neighboring triangles of T_p, and the wide one which uses all the triangles with a common vertex with T_p (Fig. 3).

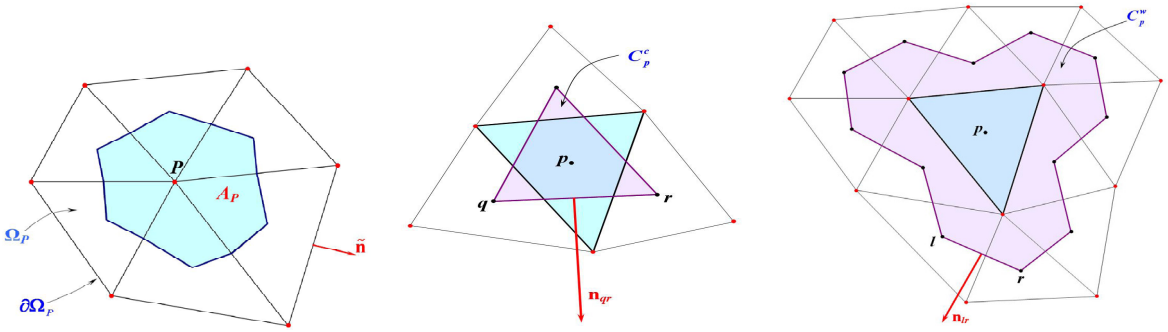

Figure 3: Stencils for gradient calculation for the NCFV (left), CCFVc2 (center) and CCFVw2 (right)

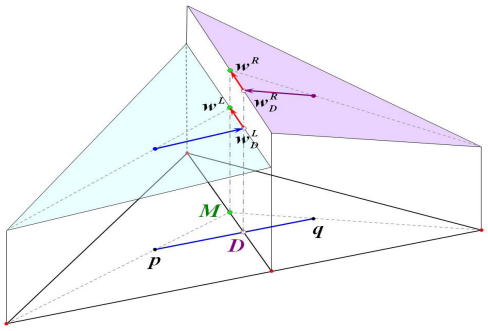

Figure 4: Proposed reconstruction for the CCFV scheme

For the boundary conditions, proper ghost cells are used for the CCFV scheme and the weak

formulation is used for the NCFV boundary nodes.

4 SOURCE TERMS AND WET/DRY FRONT TREATMENT

While the C-property holds for the 1st order schemes, i.e. if the L and R values are not reconstructed, this is not the case for the second order MUSCL discretization. As such, and following[6] for the CCVF approach and[2] for the NCFV approach, a term is added to the source term discretization for maintaining the correct balance.

In the boundary defined by a wet/dry front a special treatment is needed in order to accurately model the transitions between wet and dry areas while at the same time maintain second order spatial accuracy. The following issues have been addressed: (a) *Identification of dry cells*: a tolerance parameter depending on the mesh characteristics is used[7]; (b) *Consistent depth reconstruction*: reconstructed values at the wet/dry interface are computed as to satisfy $\nabla h = -\nabla B$; (c) *Conservation of the flow at rest with dry regions*: The bed slope in the computation of $\mathbf{\Psi}$ in (7) is redefined[3] as to satisfy an extended C-property[1,2]; (d) *Flow in motion over adverse slope*: Applying the redefinition in (c) then the numerical fluxes at the wet/dry interface are computed assuming temporarily zero velocity[1,2]; (e) *Mass conservation*: The error due to possible negative depths or due to the imposed threshold are summed and added properly into the entire computational domain[4,8].

In order to handle the friction terms in (4) a separate implicit formulation[4] was applied inside a 4-step, 2nd order Runge-Kutta method used for time marching[2].

5 NUMERICAL RESULTS AND DISCUSSION

We first consider a particular member of a family of 2D exact potential solutions, which satisfies the frictionless steady state over topography[7,8]. The convergence results for the 4 different types of grids and for the three schemes are presented in Fig. 5. For the NCFV scheme all 4 grids provided identical convergence results with a rate higher than 2, demonstrating the independence of the corresponding scheme from the grid type used. For the CCFVc2 (compact gradient stencil with the proposed modified reconstruction) all grids provided almost identical slopes but for two of them (III and IV) higher errors were obtained. These differences are attributed to the numerical boundary conditions (implemented using ghost cells), where large distances between points D, M (Fig. 4) are present (especially for type III). The convergence slopes for the CCFVw2 scheme (wide gradient stencil with the proposed modified reconstruction) are higher, compared to the CCFVc2 case, which is attributed to the fact that the large gradient stencil allows for a more accurate computation of the (unlimited) additional terms in Eq. (10). The results concerning type III grid are not improved, as the compact gradient stencil is always used on the boundary triangles even for CCFVw2 scheme. Similar convergence results were obtained respectively for the hu, hv conserved variables.

The second case considered is Thacker's planar analytic solution[2] which includes wetting and drying, and the corresponding convergence results are exposed in Fig. 6. Similarly to the first case, for the NCFV scheme all 4 grids provided identical convergence results, with a mean rate around 2. For the CCFVc2 scheme type II, III grids resulted in higher errors than I,

IV grids, which are reduced with the CCFVw2 scheme, for the same reason as for the first case considered. The higher errors of type II grid are due to the large distance between points *D*, *M* for this type of grid. We note here that, for both test cases considered, the differences between the asymptotic rate of convergence for the various types of girds for the CCFV schemes (compact and wide) without using the proposed modification in gradient reconstruction (Eq. 10) were much more pronounced (not shown here for brevity).

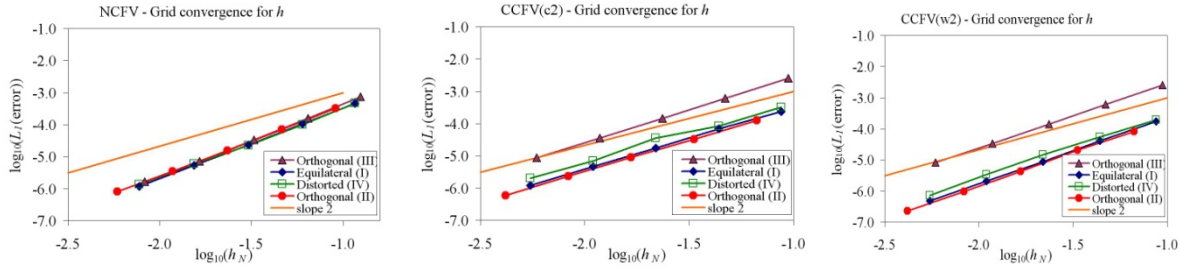

Figure 5: Convergence results for the 2D potential steady state case over topography (L_1 norm).

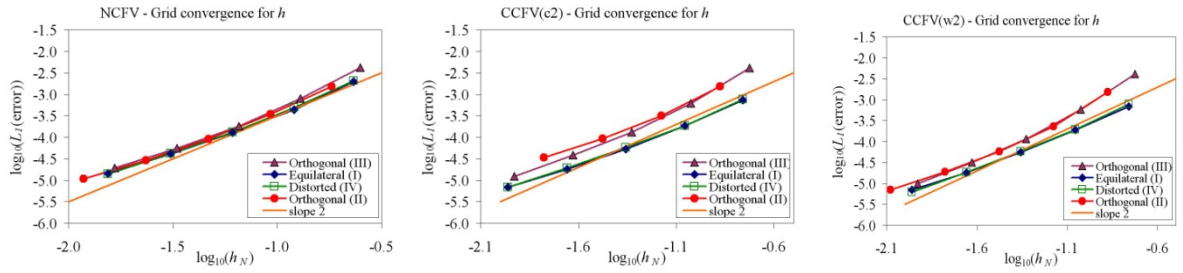

Figure 6: Convergence results for the Thacker's planar case (L_1 norm).

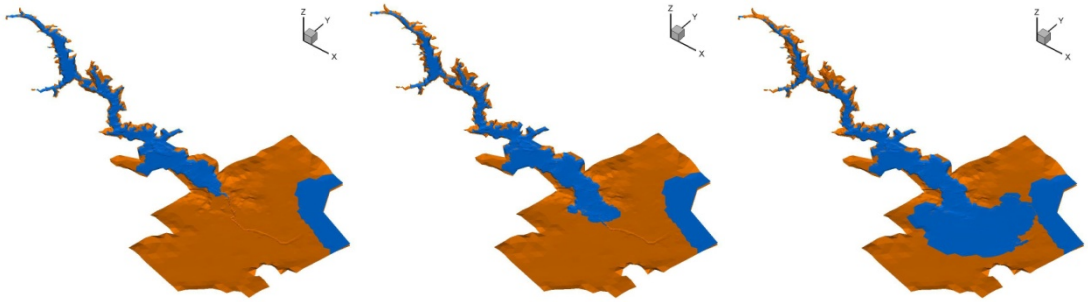

Figure 7: Simulation for the Malpasset case with the NCFV scheme, at times 1200, 1600, and 2400sec.

The simulation of Malpassed[4] dam breach was used to evaluate the differences of the three schemes in a field test case. Fig. 7 contains simulation results using the NCFV scheme. The corresponding results for the two CCFV schemes were almost identical. All simulations have been conducted with the same triangular grid (provided by EDF) and n_m=0.033. Comparisons with measured data, concerning water arrival times to the positions of three electric transformers, and the maximum free surface elevation at certain positions measured by the

police, are presented in Fig. 8. All three schemes provided accurate and comparable results, with the NCFV scheme showing slightly better agreement with the field data, although the results were obtained with half the degrees of freedom of the CCFV schemes (corresponding to a much lower computation time). Taking also into account the simplicity in the implementation of boundary conditions (without the use of ghost cells), and its independence from the grid type (for the typical grids used), the NCFV scheme seems to be a better choice for the type of problems considered in this work.

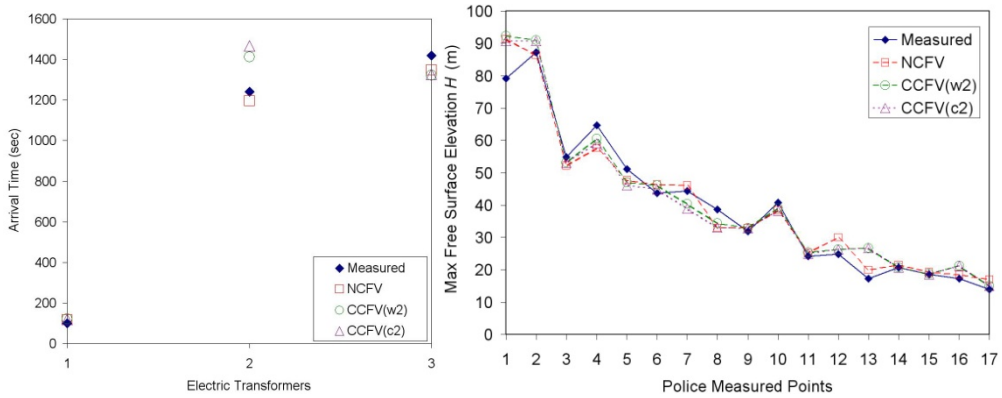

Figure 8: Comparisons with measured data for the Malpasset field test case.

REFERENCES

[1] A.I. Delis, M. Kazolea, and N.A. Kampanis, "A robust high resolution finite volume scheme for the simulation of long waves over complex domain", *Int. J. Numer. Meth. Fluids*, **56**, 419 (2008).

[2] I.K. Nikolos and A.I. Delis, "An unstructured node-centered finite volume scheme for shallow water flows with wet/dry fronts over complex topography", *Comput. Methods Appl. Mech. Engrg*, **198**, 222 (2009).

[3] P. Brufau, M.E. Vazquez-Cendon, and P. Gracia-Navarro, "A numerical model for the flooding and drying of irregular domain", *Int. J. Numer. Meth. Fluids*, **39**, 247 (2002).

[4] P. Brufau, P. Garcia-Navarro, and M.E. Vazquez-Cendon, "Zero mass error using unsteady wetting-drying conditions in shallow flows over dry irregular topography", *Int. J. Numer. Meth. Fluids*, **45**, 1047 (2004).

[5] A. Bermudez, A. Dervieux, J.A. Desideri, and M.E. Vazquez, "Upwind schemes for the two dimensional shallow water equations with variable depth using unstructured meshes", *Computer Methods in Applied Mechanics and Engineering*, **155**, 49 (1998).

[6] M.E. Hubbard and P. Garcia-Navarro, "Flux difference splitting and the balancing of source terms and flux gradients", *J. Comp. Phys.*, **165**, 2 (2000).

[7] M. Ricchiuto and A. Bollermann, "Stabilized residual distribution for shallow water simulations", *J. Comp. Phys.,* **1071**, 1115 (2009).

[8] A.I. Delis, I.K. Nikolos, and M. Kazolea, "Comparison of cell-centered and node-centered unstructured finite volume discretizations for shallow water free surface flows" (submitted).